



Photodegradation of Direct Violet 51 Dye using $\text{Bi}_2\text{MoO}_6/\text{GO}$ Nanoflakes as Promising Solar Light-driven Photocatalyst

Sumaira Younis^{1,2}, Haq Nawaz Bhatti^{1*}, Sadia Z. Bajwa², Jie Xu³, and Saba Jamil¹

¹Department of Chemistry, University of Agriculture, Faisalabad, Pakistan

²Nanobiotech Group, National Institute for Biotechnology and Genetic Engineering (NIBGE), Jhang Road, Faisalabad, Pakistan

³Department of Mechanical and Industrial Engineering, College of Engineering, University of Illinois at Chicago, Chicago, USA

Abstract: Water contamination is a challenging issue for the maintenance of environmental sustainability. Industrial effluents are considered major sources of water pollution which affect the quality of surface as well as ground water. In the present research work, semiconducting Bismuth Molybdate/Graphene Oxide ($\text{Bi}_2\text{MoO}_6/\text{GO}$) composite nanomaterial has been introduced as the solar light-driven catalyst for photodegradation of Direct Violet (DV) 51 dye and industrial wastewater. Scanning electron microscope (SEM), zeta potential, X-ray diffraction analysis and Fourier transform infrared spectroscopy (FTIR) were used to characterize the $\text{Bi}_2\text{MoO}_6/\text{GO}$ composite material. Experimental findings revealed that flake-like $\text{Bi}_2\text{MoO}_6/\text{GO}$ composite exhibits 99.00 % degradation activity against DV dye within 80 minutes. $\text{Bi}_2\text{MoO}_6/\text{GO}$ nanoflakes degrade DV dye up to 98.70 % at pH 7 and 99.99 % with a 100 mg catalyst dose within 60 minutes, respectively. The stability/reusability study presented 99.82 % - 93.84 % dye degradation from the 1st to 7th day within 80 minutes while optimizing experimental parameters. According to kinetic studies of experimental outcomes, the pseudo-first-order model was best fitted to the obtained data with a coefficient of determination $R^2=0.954$. Moreover, a 69.23 % reduction was observed in chemical oxygen demand (COD) during the photodegradation study of industrial wastewater. Results indicate that $\text{Bi}_2\text{MoO}_6/\text{GO}$ nanoflakes have good photocatalytic potential and stability to degrade organic water pollutants under sunlight. Such materials can be used effectively for the photodegradation of organic water pollutants to enhance environmental safety.

Keywords: Water pollution, Direct violet 51 dye, Photodegradation, Graphene oxide (GO), Bismuth molybdate (Bi_2MoO_6).

1. INTRODUCTION

Water pollution has become a severe ecological threat globally, it requires due attention to maintain a healthy lifestyle. There are a variety of organic pollutants like dyes, pesticides, fungicides, drugs, and food toxins in environmental components such as soil, water, crops, vegetables, fruits, and juices, etc. which exert undesirable effects on the human as well as other living creatures [1]. Their release into water systems badly disturbs the quality of both ground and surface water leading to critical health issues in living beings. Due to their non-

biodegradable nature and long-range transport, they accumulate in living tissues and disturb the food chain [2]. Among the released waste products into water bodies, dyes are considered as coloring materials having potential applications in multiple fields like textile, leather, plastics, paper, precious stones, food products, etc. The addition of such complex organic compounds into water bodies inhibits solar light transmission and affects aquatic life. On average there are about more than one hundred thousand synthetic dyes having an estimated production of seven hundred thousand tons/annum throughout the world, resulting in

substantial production of wastewater [3].

Direct violet 51 dye is found in the class of direct dyes including water-soluble anionic azo dyes. According to the Santa Cruz Biotechnology, Inc. supplier's safety data sheet, Direct violet 51 is a synthetic, anionic dye having double azo groups. These azo groups act as chromophores to impart color in the textile, paper, and leather industries. Metabolism of azo groups prone to produce carcinogenic aromatic amines such as benzidine. Complex direct dyes have more than one azo linkage and their ingestion or contact may lead to mutagenic, cardiogenic, chronic bronchitis, vomiting, nausea as well as skin, eye, and respiratory tract irritation in humans. In aquatic media, they block the penetration of sunlight and interrupt the photosynthesis in aquatic plants leading to disturb marine life [4].

Removal of such toxic pollutants is a critical situation for the environment and the agencies related to it. A lot of work has been conducted in this area using conventional techniques like filtration, sedimentation, coagulation, membrane separation, flocculation, and adsorption, etc. No doubt these techniques have their importance but also have some limitations i.e., laborious, time taking, high consumption of chemical reagents and transform the pollutants from one phase to another by generating secondary pollutants which result in incomplete removal of toxic substances [2]. Among these progressions, heterogeneous photocatalysis has attracted much attention as a facile and cost-effective method. It is a well-known advanced oxidation method that utilizes light-sensitive photocatalysts to accelerate photochemical reactions by harvesting solar energy and results in the complete degradation of organic pollutants without generating secondary pollutants [5, 6].

Growing complications in environmental pollution draw considerable attention to searching nanomaterials bearing multiple catalytic potentials. Their significance increases due to the highly efficient mode of action and cost-effectiveness than conventional techniques [7]. Semiconducting metal oxides and their composites with carbon-based nanostructures have fascinating photocatalytic applications due to their synergistic effects. Two-dimensional (2D) materials (nanosheets, nanoplates, nanoflakes, etc.) play a major role in

photocatalytic applications due to their outstanding properties, offering large interlayer spaces and high active surface area owing to more exposed surface atoms. Their flattened and thinner dimensions provide multiple pathways for the migration of charge carriers augmenting the photocatalytic potential at the atomic level [8].

2D Graphene oxide (GO) has outstanding electrochemical characteristics due to its electron promotor attributes. The presence of reactive oxygenated functional groups provides stable chemical reactivity as a catalyst as well as for the formation of composite materials with other metallic nanostructures to overcome the recombination of charge carriers during photocatalysis [9]. Bismuth molybdate (Bi_2MoO_6) belongs to the family of Aurivillius oxide perovskites. Bi_2MoO_6 is a very stable semiconductor material offering good photocatalytic activity due to its perovskite layered structure. Its crystal structure has corner-sharing MoO_6^{2-} octahedrons sandwiched between alternating $\text{Bi}_2\text{O}_2^{2+}$ layers providing a large active surface area for the effective separation of charge carriers [10, 11].

In the present study, we introduced the synthesis and application of Bi_2MoO_6 /GO nanoflakes. GO was synthesized by Hummer's method while Bi_2MoO_6 /GO composite nanoflakes were developed through a hydrothermal route. The synthesized Bi_2MoO_6 /GO composite nanoflakes were applied as solar light-driven nano-photocatalysts to degrade Direct violet 51 dye, a model organic water pollutant. To study the real-life application of these nano-photocatalysts, industrial wastewater was also treated with composite nanoflakes under sunlight. Experimental outcomes revealed excellent photodegradation efficiency of Bi_2MoO_6 /GO nanoflakes against model dye and industrial wastewater by harvesting solar energy. According to the author's knowledge, there is no elaborated work on the photodegradation of direct violet 51 dye by using Bi_2MoO_6 /GO composite as a photocatalyst.

2. MATERIALS AND METHODS

2.1 Chemicals/Reagents

Chemicals and reagents i.e. hydrogen peroxide (H_2O_2 , 35 %, BDH), graphite powder

(98.0 % UNI-CHEM), sodium hydroxide (NaOH, 98-100 %, Sigma Aldrich), sulphuric acid (H_2SO_4 , 98 %, Merck), methanol (99.5 %), ethanol (99.8 %), sodium molybdate dihydrate ($\text{NaMoO}_4 \cdot 2\text{H}_2\text{O}$, ≥ 99.5 %), acetic acid (CH_3COOH , 99 %, Merck), bismuth nitrate pentahydrate [$\text{Bi}(\text{NO}_3)_3 \cdot 5\text{H}_2\text{O}$, 98 % Merck], potassium permanganate (KMnO_4 , 99 %, RFCL) hydrochloric acid (HCl , 36.5-38 %, Sigma Aldrich), and sodium nitrate (NaNO_3 , ≥ 99.0 %, Merck) were used as such without any treatment. Deionized water (DI) was used as a solvent for the preparation of solutions obtained from the Millipore-MilliQ system.

2.2 Production of Graphene oxide (GO)

Modified Hummer's method was used to synthesize graphene oxide (GO) by the oxidation of graphite [12]. In a typical synthetic route graphite powder and sodium nitrate were added in a 6:3 ratio to the concentrated sulphuric acid (200 mL) in the ice bath at constant stirring. After 25 minutes potassium permanganate (40 g) was added slowly on vigorous stirring by maintaining the solution temperature below 15 °C for 2 hours. To obtain a brownish dense slurry the reaction media was kept on constant stirring at 30-35 °C for 36-48 hours. Then deionized water was added slowly, temperature of the reaction medium was raised to 90 °C and maintained at this temperature for about 25-30 minutes. The suspension was cooled down at room temperature and 60 mL H_2O_2 was added dropwise on constant stirring to stop the reaction. After 10 minutes, 10 percent HCl was added to the suspension and allowed to settle down brownish GO precipitates for 24 hours, GO precipitates were collected, methanol, and deionized water were used as washing solvents to eliminate the impurities from the final product and desiccated at 60 °C under vacuum.

2.3 Synthesis of Bismuth Molybdate graphene oxide (Bi_2MoO_6)/GO composite nanoflakes

A facile hydrothermal method was used to synthesize (Bi_2MoO_6)/GO nanoflakes. For this, a 40 mL sodium molybdate dihydrate ($\text{NaMoO}_4 \cdot 2\text{H}_2\text{O}$) solution (0.07 M) was prepared in DI water termed as (A). Meanwhile, 20 mL 0.1M bismuth nitrate pentahydrate was dissolved in 2.5 M acetic acid on constant stirring as the solution (B). Graphene oxide (GO) 40 mg was dispersed in 20 mL of

deionized water via sonication. Solution (A) was added to the solution (B) dropwise on continuous stirring. Consequently, graphene oxide suspension was added to the resulting suspension and left on continuous stirring for 30 minutes. Then this suspension was poured into a 200 mL stainless steel, Teflon-lined autoclave to place in a heating oven at 180 °C for 16 hours. After completion of the reaction time, the autoclave was cooled down at room temperature. (Bi_2MoO_6)/GO product was collected, washed with absolute ethanol, and deionized water to purify the material. The obtained material was dried in the heating oven at 80 °C for 6 hours. The dried material was ground to a fine powder and stored in an airtight jar.

2.4 Characterization

Scanning electron microscope Raith-e-Line was used to investigate the morphology of prepared nanostructures. For SEM analysis, the suspension was prepared by dispersing 1 mg of (Bi_2MoO_6)/GO material in 2 mL absolute ethanol via sonication. 20 μL suspension was spin-coated on carbon-coated copper grids and allowed to dry to obtain a stabilized layer. Phase purity and crystal structure were determined by X-ray diffraction technique. The spectra were recorded in the 2-theta range of 10-90 ° on Bruker D8 Discover X-ray Diffraction System with $\text{Cu K}\alpha$ radiation i.e. $\lambda=0.15406$. Zeta Sizer Nano Series from Malvern Instruments was used to estimate the zeta potential/surface charge of the as synthesized (Bi_2MoO_6)/GO material. To determine the active functional groups in the obtained composite, the material was analyzed through Fourier transform Infrared spectroscopy using Cary-630 Fourier transform Infrared spectroscope in ATR (attenuated total reflection) mode.

2.5 Application of Nanomaterials as Photocatalysts

To study the photocatalytic degradation activity of synthesized (Bi_2MoO_6)/GO nanostructures against model dye, solar light was used as an irradiation light source to accelerate the nanomaterials as photocatalysts. 1000 ppm stock solution of direct violet 51 (DV) dye was prepared by adding 0.1 g of DV in 1000 mL deionized water. Then further dilutions (10-100) ppm were prepared from the stock solution by using the dilution formula.

To see the effect of contact time and kinetic study 50 mg (Bi_2MoO_6)/GO nanostructures were added in 20 ppm, 50 mL Direct violet 51 (DV) dye solution and kept in dark for a half hour for maintaining adsorption and desorption equilibrium of dye molecules on the surface of nanostructures. Then subjected to solar light for different time intervals (0-80 minutes). The rate of dye degradation by nanostructures was determined by evaluating the decrease in the relative maximum absorbance at the characteristic wavelength ($\lambda_{\text{max}} = 586 \text{ nm}$) of the dye solution. For this, after regular time intervals 3 mL solution of direct violet 51 dye was taken out and centrifuged at 500 rpm to separate any suspended nanostructures and the intensity of relative absorbance at 586 nm was measured by UV/Visible spectrophotometer.

To study the effect of pH 0.1 M HNO_3 and 0.1 M NaOH solutions were utilized to adjust the pH of dye solution from 3-9. 20 mg of nanostructures were added in dye solutions having the same concentration (20 ppm), equal volume (20 mL) but different pH (3-9), and subjected to sunlight for 1 hour. To see the reusability and stability, (Bi_2MoO_6)/GO photocatalysts were used again and again to degrade the respective new dye solution of the same concentration. For this, the (Bi_2MoO_6)/GO nanostructures were collected by centrifugation from treated dye solutions, washed with ethanol and deionized water to remove any residual dye molecule, dry at 60-80 °C for 4-6 hours. After complete drying, the nanocatalysts were again added into the fresh dye solution of the same concentration (20 ppm) and equal volume (20 mL) under vigorous stirring in dark for a half hour and then subjected to solar light for respected time e.g. 60 minutes. The concentration of residual dye was observed by recording the difference in absorbance of respected maximum wavelength ($\lambda_{\text{max}} = 586 \text{ nm}$) through UV/Vis spectrophotometer to see the difference in % degradation. The percentage degradation of model dye was assessed through the given formula.

$$\% \text{ degradation} = \frac{C_0 - C_t}{C_0} \times 100$$

Here, “ C_0 ” denoted the initial dye concentration at time (t)=0, while “ C_t ” is the dye concentration after treatment with photocatalysts at a given time ($t = 10, 20, 30, 80 \text{ minutes, etc.}$).

2.6 Chemical Oxygen Demand (COD)

For the real-life application of as synthesized nanostructures, industrial wastewater containing various dyes was treated with (Bi_2MoO_6)/GO composite. Chemical oxygen demand (COD) was calculated to check the degradation efficacy of nanostructures against organic matter in wastewater. [13]. Three working solutions were used during the experimental study of chemical oxygen demand. Digestion solution (70 mM Potassium dichromate), 200 ppm potassium hydrogen phthalate (KPH) standard solution, and 5 g $\text{AgSO}_4 / 500 \text{ mL}$ of Concentrated Sulphuric acid were used as catalyst solution.

Three test tubes were used in triplicate, e.g., three test tubes were marked as blank, three for standards and three for sample solution, for triplicate run respectively. Catalyst solution (2.8 Ml) and 1.2 mL of digestion solution were poured into all test tubes. For blank, 2 mL deionized water, 2 mL KPH as the standard solution, and 2 mL industrial wastewater as standard, and the sample was added in separate test tubes in triplicate, respectively. All test tubes were refluxed well to homogenize the mixtures and then placed in a heating reactor at 150 °C for two hours. After this, test tubes were cooled down at room temperature for 30 minutes, and recorded the absorbance of treated blank, standard, and sample solution was at a wavelength of 600 nm via spectrophotometer. The difference in chemical oxygen demand before and after treatment was calculated using the formula;

$$\text{Chemical oxygen demand} = \text{standard factor} \times \text{optical density}$$

$$\text{COD removal (\%)} = \frac{\text{Initial COD} - \text{Final COD}}{\text{Initial COD}} \times 100$$

3. RESULTS AND DISCUSSION

3.1 Possible Growth Mechanism of $\text{Bi}_2\text{MoO}_6 / \text{GO}$ Nanocomposite

During hydrothermal growth reactions, Bi_2MoO_6 crystals were formed in 2 steps (1) Bismuth ions (Bi^{3+}) interacted with water molecule/OH-groups and converted into the $\text{Bi}_2\text{O}_2^{2+}$ ionic layers. (2) $\text{Bi}_2\text{O}_2^{2+}$ ionic layers interact with MoO_4^{2-} ions

and are converted into Bi_2MoO_6 nuclei and then arranged into a specified flake-like shape according to the reaction conditions. Graphene oxide interacts with Bi_2MoO_6 nuclei through the electrostatic or hydrogen bonding forces leading to the formation of $\text{Bi}_2\text{MoO}_6/\text{GO}$ nanocomposite material. The presence of oxygenated functional groups in GO plays a major role in its chemical reactivity towards other nanostructures [14].

3.2 Morphology and Structural Analysis of $\text{Bi}_2\text{MoO}_6/\text{GO}$ Nanocomposite

Morphology of graphene oxide (GO) and $\text{Bi}_2\text{MoO}_6/\text{GO}$ composite was evaluated by scanning electron microscopy. Figure 1 (A) shows the flattened, thin sheet-like morphology of graphene oxide nanosheets. GO has crumpled, layered morphology. Ultra-thin GO sheets are rippled and entangled with each other having randomly oriented corners or edges. SEM analysis of $\text{Bi}_2\text{MoO}_6/\text{GO}$ nanomaterial shows the high yield of 2D flake-like morphology having different size and shape distribution. Nanoflakes have flattened surfaces with zigzag margins. It was also observed that the nanoflakes have one broader and other least broadened ends. Nanoflake's analysis through Image J. software revealed that they have a thickness of around 40-50 nm, width and height were observed to be more than 200 nm. The flattened surface plays a major role in increasing the active surface area of 2D nanomaterials as shown in Figure 1 (B).

Structural and functional characterization of $\text{Bi}_2\text{MoO}_6/\text{GO}$ nanoflakes is shown in Figure 2. The crystallinity and phase purity of the composite material was analyzed through a powder X-ray diffraction study. XRD analysis revealed the composition of nanoflakes as bismuth molybdate according to the given Empirical and Chemical formulae: Bi_2MoO_6 . All diffraction peaks in the XRD pattern were found to be well indexed to the orthorhombic crystalline structure with lattice parameters $a=5.5060$ (Å), $b=16.2260$ (Å), and $c=5.4870$ (Å) with JCPDS Card No. 01-072-1524.

The diffraction peaks were detected at 2-theta values of 11.1° , 14.5° , 19.6° , 26.5° , 28.5° , 32.5° , 35.2° , 46.71° , 51.15° , 52.31° , 55.40° , 58.44° , 75.66° , and 86.80° correspond to (020), (021), (040), (121), (131), (002), (022), (152), (023), (024), (262), (333) and (462) hkl planes of nanoflakes (Figure 2 A). The sharp and intense peaks illustrate that the sample is well crystallized even in composite form with GO. There was no specific peak for GO which might be due to less concentration of GO as compared to Bi_2MoO_6 . The superior relative intensity of the (131) diffraction peak at 28.5° exhibits the (131) preferred orientation in the $\text{Bi}_2\text{MoO}_6/\text{GO}$ nanoflakes [15].

FTIR profile of the $\text{Bi}_2\text{MoO}_6/\text{GO}$ nanoflakes shows the structural functionalities in Figure 2(B). The band that appears at 3468 cm^{-1} might be assigned to O-H bonds stretching vibrations. The

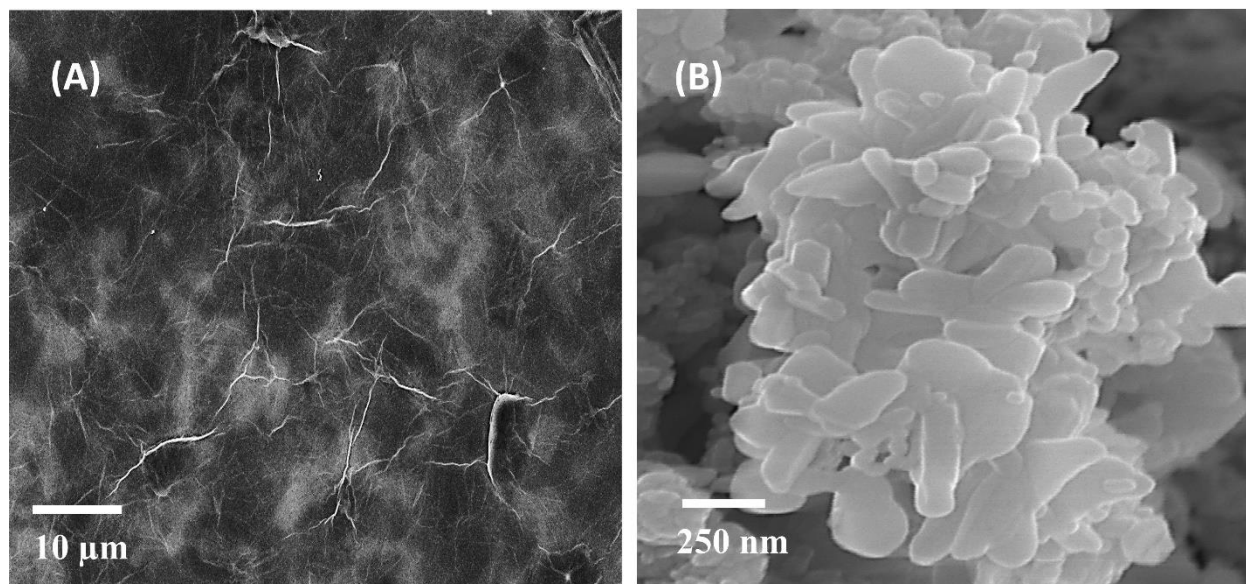


Fig. 1. SEM images showing morphological characterization of GO (A) and $\text{Bi}_2\text{MoO}_6/\text{GO}$ nanoflakes (B).

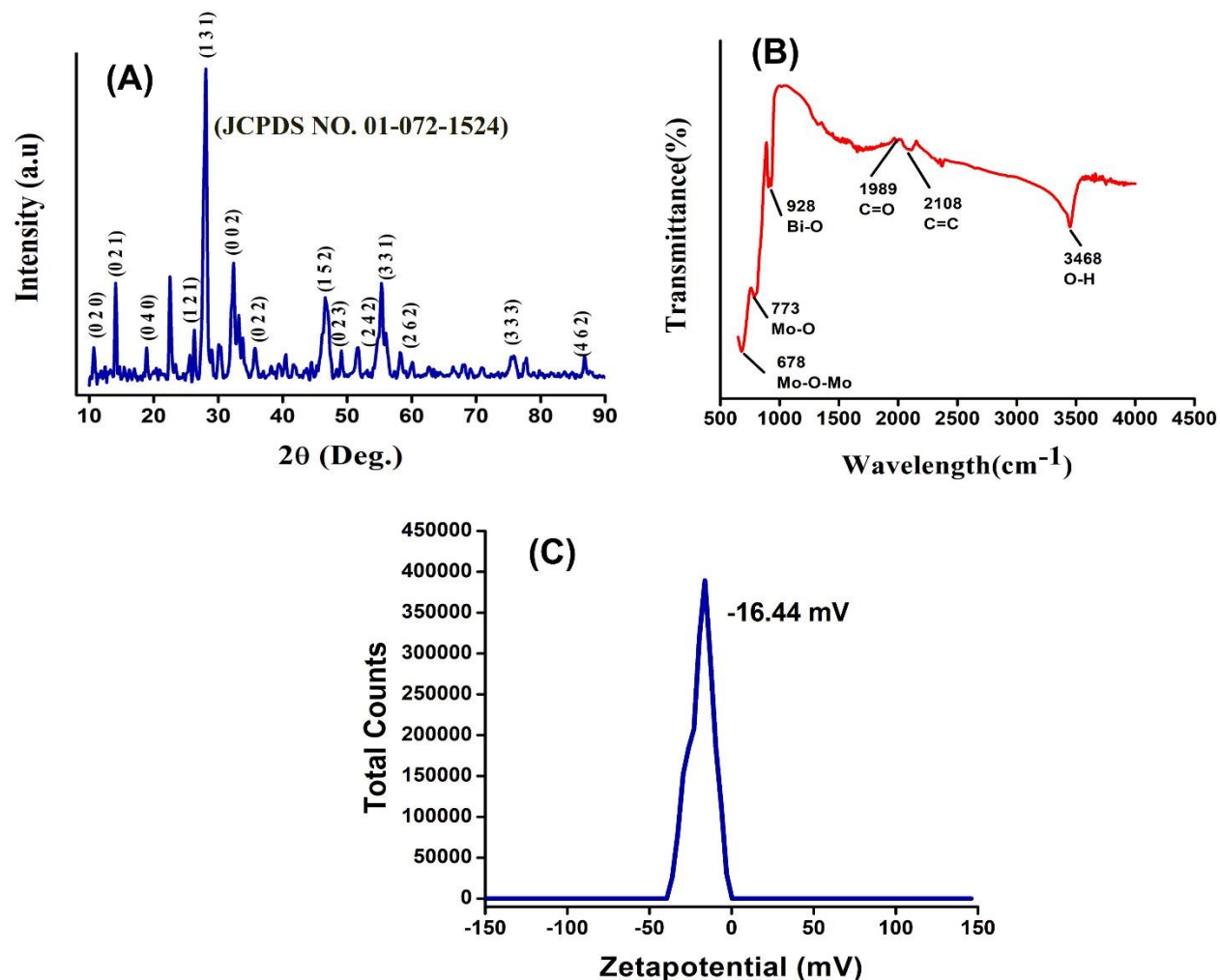


Fig. 2. Structural and functional characterization of $\text{Bi}_2\text{MoO}_6/\text{GO}$ nanoflakes. XRD pattern displaying phase purity (A), FTIR Profile (B), Zeta surface potential scan (C).

two consecutive bands appearing at about 1988 and 2108 can be attributed to the C=O bending vibrations of carboxyl groups and aromatic C=C bending vibrations in GO respectively. The bands centered at 980 cm^{-1} and 773 cm^{-1} were assigned to the stretching vibrations of Bi-O and Mo-O respectively. Another band appearing at 678 cm^{-1} was well indexed to bridging stretching vibrations of Mo-O-Mo bonds [15]. Figure 2(C) shows the zeta potential analysis of the $\text{Bi}_2\text{MoO}_6/\text{GO}$ nanoflakes. The surface charge was found to be -16.44 mV revealing that the material is negatively charged. Surface charge plays an important role in the colloidal stability of the nanomaterial [16, 17].

3.3 Photocatalytic Degradation of Direct Violet (DV) dye by $\text{Bi}_2\text{MoO}_6/\text{GO}$ nanoflakes

The solar light harvesting photocatalytic efficiency

of $\text{Bi}_2\text{MoO}_6/\text{GO}$ nanoflakes was estimated against the photodegradation of Direct Violet (DV) dye as a model organic water pollutant. The absorption spectra of the under-test DV dye solution was recorded from 400-800 nm and the characteristic maximum absorbance was observed at 586 nm. Bi_2MoO_6 nanostructures are used as good photocatalysts for the degradation of organic water pollutants due to narrow bandgap i.e. 2.5-2.8 [18]. Recombination chances of electron-hole pairs can also occur during the excitation of an electron from the conduction band (CB) to the valence band (VB) which can slow down or stop the photocatalytic reaction. Addition of GO with Bi_2MoO_6 provides an effective charge transfer and causes a reduction in the recombination of electron-hole pairs. The conduction band (CB) of $\text{Bi}_2\text{MoO}_6/\text{GO}$ is composed of Bi, 6p, and Mo 4p molecular orbitals whereas O 2p orbitals made the valence band (VB). GO

behave as an electron promoter by minimizing the back transfer of excited electrons and facilitates a continuous oxidation process [19].

During the photocatalysis process semiconductor $\text{Bi}_2\text{MoO}_6/\text{GO}$ photocatalyst absorbs photons of energy equivalent to its band gap energy. Absorption of photons leads to the excitation of electrons from the valence band to conduction band of the catalyst by leaving a hole in the valence band. Graphene oxide captures the excited electrons from the conduction band of Bi_2MoO_6 preventing the recombination of generated electron-hole pairs, leading to the formation of superoxide ($\text{O}_2^{\cdot-}$) and hydroxy radicals. The holes in the valence band lead to the formation of hydroxyl ($\cdot\text{OH}$) radicals. Superoxide and hydroxyl radicals behave as strong oxidizing and reducing agents to decompose the complex dye molecules into nontoxic constituents [17, 20] as shown in Figure 3.

3.3.1 Effect of Contact Time

To evaluate the effect of time for maximum degradation of direct violet 51 (DV) dye, absorption of dye solution was evaluated after regular time

intervals starting from 0-80 minutes without using any oxidizing agent to accelerate the degradation process. The characteristic absorbance at 586 nm of DV in an aqueous solution decreases more quickly under the degradation activity of the photocatalyst. Figure 4(A) shows the decrease in the absorbance of respective wavelength ($\lambda_{\text{max}} = 586 \text{ nm}$) for DV dye (20 ppm) aqueous solution (50 mL) with 50 mg of $\text{Bi}_2\text{MoO}_6/\text{GO}$ nanoflakes as photocatalyst. Figure 4 (B) shows the percent degradation of DV dye solution as a function of contact time. Results indicate that there is around 19.22 % elimination of dye was due to adsorption even at the time of adsorption-desorption equilibrium in dark. After the interaction with sunlight dye color starts to become fade showing the degradation of dye molecules. There is a gradual increase in the degradation rate up to 50 minutes which results in 97.94 % dye degradation and then the degradation rate became slow down and give 99.00 % degradation within the test period up to 80 minutes.

3.3.2 Effect of pH

pH of aqueous solution also affects the photocatalytic activity of catalysts. pH affects the surface charge

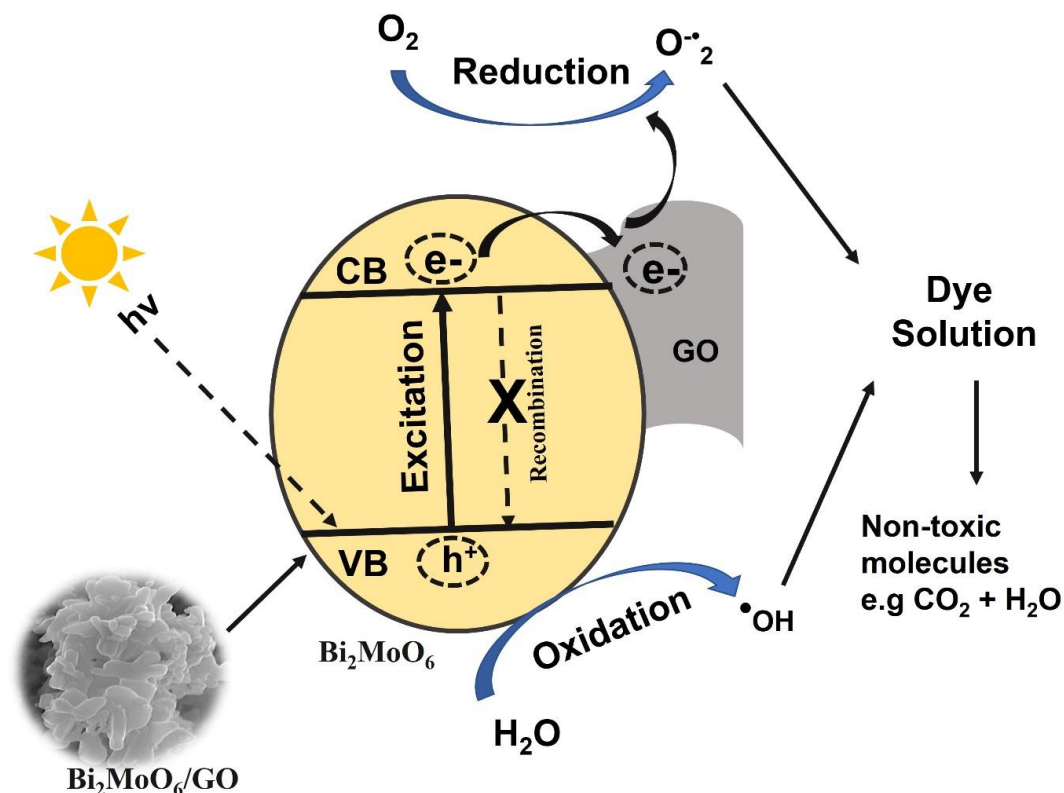


Fig. 3. Photocatalysis mechanism of $\text{Bi}_2\text{MoO}_6/\text{GO}$ nanoflakes for photodegradation of direct violet 51 dye under solar energy.

of catalysts according to their point of zero charges (pHPZC) and results in to change in the adsorption capacity of catalysts [21]. To see the pH effect of aqueous DV dye solutions on the photocatalytic efficiency of $\text{Bi}_2\text{MoO}_6/\text{GO}$ nanoflakes, the pH of dye solutions was adjusted by using 0.1 M NaOH and 0.1 M HNO_3 from 3-9. Other experimental conditions were the same, e.g dye concentration (20 ppm), volume (20 mL), catalyst dose (20 mg), and time was 60 minutes. An increase in pH from 3-7 exhibits increase in the degradation rate of dye molecules (76.14-98.70 %) and then a decrease in % degradation at pH 9 (86.82 %). Results indicate that maximum dye degradation of about 98.70 % was observed at neutral pH=7 rather than acidic and basic pH (Figures 4C and D). This phenomenon may be because at acidic pH more hydronium ions surrounds negatively charged catalyst and reduce the interactions of anionic DV dye molecules leading to a slow-down dye degradation rate. By increasing the pH value, the number of hydronium ions decreases, and the interaction of dye molecules increases towards $\text{Bi}_2\text{MoO}_6/\text{GO}$ nanoflakes

photocatalyst leading to a higher dye degradation rate by the rapid formation of hydroxyl radicals. Further increase in pH =9, has a negative effect on the degradation process. This may be due to the fact that at basic pH more number of hydroxyl groups of basic dye solution suppresses the oxidation of water and dye molecules to generate the hydroxyl radicals. In an alkaline medium, both negatively charged catalyst and anionic dye molecules may repel each other and cause a decline in the degradation process [22].

3.3.3 Effect of Catalyst Dose

The amount of catalyst is also considered a function of the degradation process. To observe the effect of catalyst dose, dye solutions having the same concentration (20 mg/L) with the same volume (20 mL) were treated with different amounts of $\text{Bi}_2\text{MoO}_6/\text{GO}$ nanoflakes i-e 5, 25, 50, 100, and 150 mg for 60 minutes. Results have shown an increase in the rate of degradation i-e 51 to 99.99 %, with the increase in catalyst dose from 5 to 100 mg of

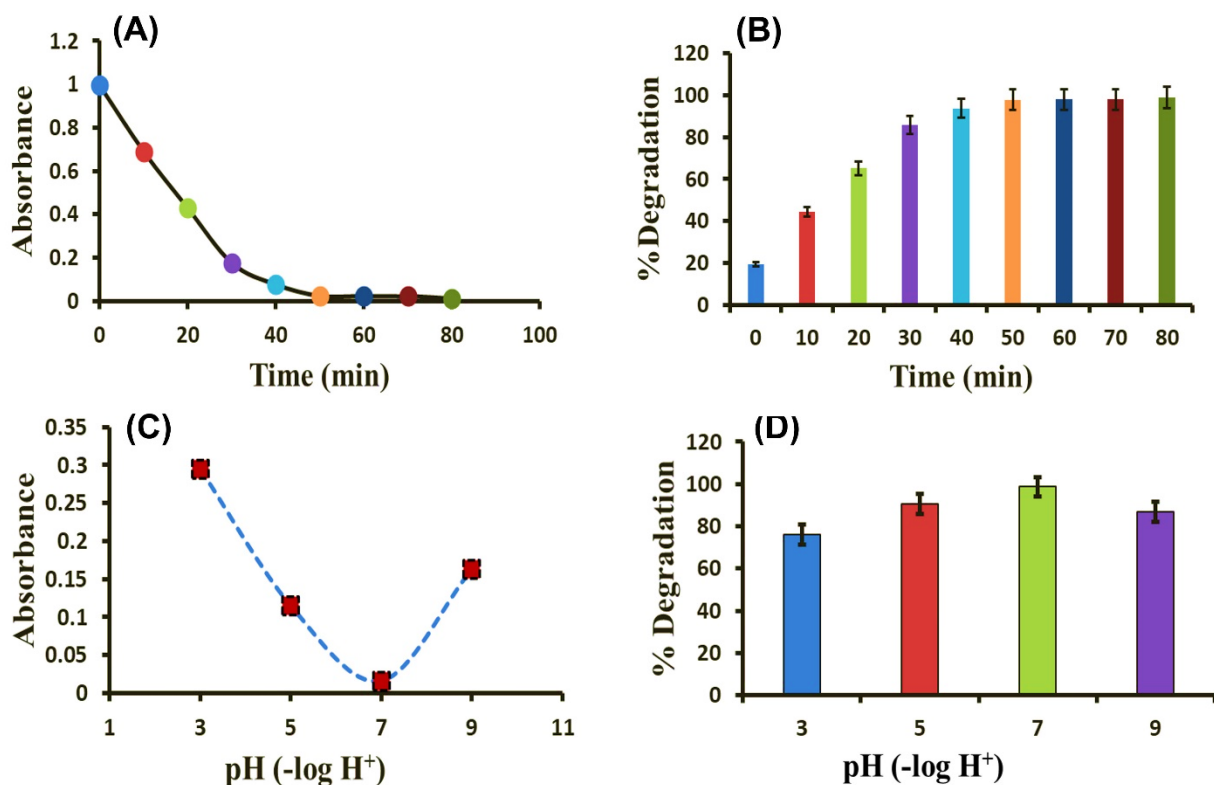


Fig. 4. Photocatalytic degradation rate of DV dye under sunlight at different time intervals with $\text{Bi}_2\text{MoO}_6/\text{GO}$ nanoflakes as the effect of contact time for experimental parameters (A), respective % degradation of DV dye at different time intervals (B), the effect of pH on degradation efficiency of $\text{Bi}_2\text{MoO}_6/\text{GO}$ nanoflakes against DV dye (C), respective % degradation efficiency of $\text{Bi}_2\text{MoO}_6/\text{GO}$ nanoflakes at different pH values of dye solution (D).

$\text{Bi}_2\text{MoO}_6/\text{GO}$ nanoflakes (Figure 5A). Further increase in the amount of catalyst about 150 mg causes an 11 % decrease in the photocatalytic activity of the catalyst. It indicates that up to a certain limit increase in catalyst dose results in the production of more reactive oxidizing species to oxidize a greater number of dye molecules in less time. In this connection, beyond the optimum catalyst dose, it has a negative effect on the degradation rate. This may be due to the agglomeration of a high dose of catalyst leading to a reduction of active surface area, or it may decrease the penetration rate of light photons to the inner layers of the dye solution. Light scattering may also occur at the surface of upper-layered $\text{Bi}_2\text{MoO}_6/\text{GO}$ nanoflakes preventing the appropriate interaction of high energy light intensity to the lower-layered catalyst surfaces [23].

3.3.4 Stability/ Reusability

In addition, to confirm the stability and reusability of the high photocatalytic performance of the $\text{Bi}_2\text{MoO}_6/\text{GO}$ nanoflakes, recycling experiments for the photodegradation of DV were conducted. For this 20 ppm, 20 mL dye solution was treated with 20 mg of catalyst for 80 minutes. The catalyst was used again and again for seven days after washing and drying to degrade the respective new 20 mL, 20 mg/L of dye solution. Figure 5 (B) exhibits 99.82 % degradation for the 1st cycle and 93.84 % dye degradation for the 7th cycle. This 5.98 % decrease in the degradation may be due to the loss of photocatalyst during centrifugation, washing, and drying procedures. It was observed

that the same catalyst can be used again and again for the degradation of organic water pollutants. Results exhibit the good stability and reusability of the used catalyst making it cost-effective without the production of side products.

3.3.5 Kinetic Modeling

Pseudo first-order kinetic model defines such type of system where the rate of degradation depends upon the extent of the molecules of dye in the solution. The linear expression for this model can be represented as.

$$\ln\left(\frac{C_0}{C_t}\right) = k_1 t$$

C_0 is the initial concentration of DV dye at the time $(t)=0$, C_t denotes the final concentration of DV after the test period $(t)=t$, k_1 is the rate constant, and “ t ” is the time of reaction. The value of the rate constant can be calculated from the slope of the plot $\ln(C_0/C_t)$ vs time (t) . Figure 6 (A) shows the plot between $\ln(C_0/C_t)$ and time (t) for DV dye when treated with $\text{Bi}_2\text{MoO}_6/\text{GO}$ nanoflakes to see the effect of contact time. The value of the coefficient of determination, $R^2 = 0.954$ which is near to unity indicates the best fitting of the pseudo 1st-order kinetic model on the data. Value of rate constant $k = 0.0587/\text{min}$. Similarly, Figure 6 (B) shows the plot between $1/C_t$ and time (t) to see the photocatalytic activity of $\text{Bi}_2\text{MoO}_6/\text{GO}$ nanoflakes for photodegradation of CV dye as a function of time to evaluate the effect of contact time. The

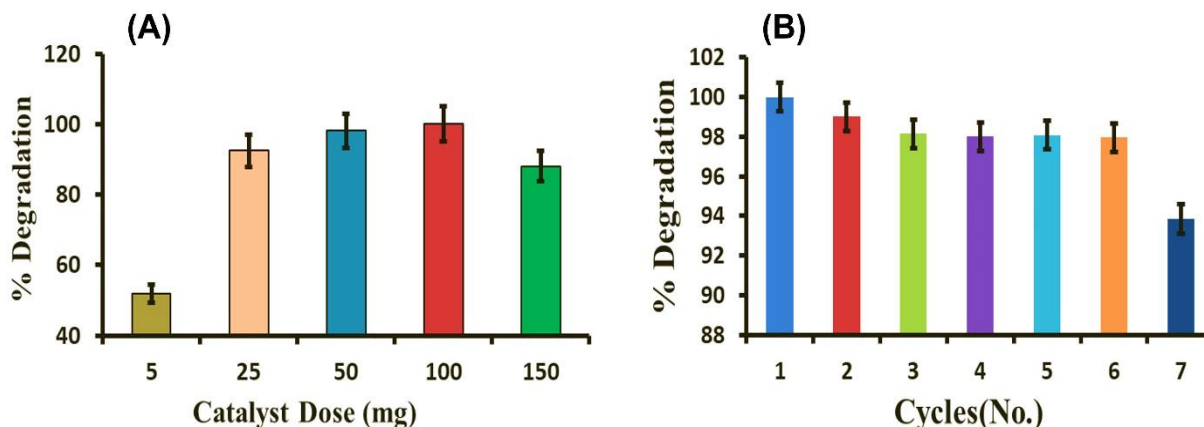


Fig. 5. % degradation of DV dye with $\text{Bi}_2\text{MoO}_6/\text{GO}$ nanoflakes for experimental parameters i.e effect of catalyst dose (A), and reusability/stability (B).

value of the coefficient of correlation shows that $R^2 = 0.84$ which is less than 0.95 (in the case of pseudo 1st order) indicating that best fitting of pseudo first order kinetic model on the dye degradation rate of reaction. Where the value of rate constant was found to be $k = 0.0587/\text{min}$ for pseudo 1st order and 0.0573 in case of pseudo 2nd-order kinetic models. The expression for the pseudo 2nd-order kinetic model is shown as

$$\frac{1}{C_t} - \frac{1}{C_0} = k_2 t$$

3.4 Chemical Oxygen Demand (COD) for Industrial wastewater treated by $\text{Bi}_2\text{MoO}_6/\text{GO}$ nanoflakes

Chemical Oxygen Demand (COD) was evaluated for industrial wastewater to check the efficacy of $\text{Bi}_2\text{MoO}_6/\text{GO}$ nanoflakes to purify industrial wastewater. For this, 20 mL of 20 times diluted industrial wastewater was treated with 20 mg of $\text{Bi}_2\text{MoO}_6/\text{GO}$ nanoflakes for 60 minutes under solar irradiation.

To see the photodegradation effect of $\text{Bi}_2\text{MoO}_6/\text{GO}$ nanoflakes against organic molecules in the sample wastewater before and after treatment COD was calculated. Initial COD value for untreated wastewater was found to be 83.85 mg/L, after treatment with a catalyst it was reduced to 25.8 mg/L.

$$\% \text{ COD removal} = \frac{(83.85 - 25.8)}{83.85} \times 100 = 69.23 \%$$

Percentage removal of COD after treatment

with $\text{Bi}_2\text{MoO}_6/\text{GO}$ nanoflakes = 69.23 %

It was found that the overall chemical oxygen demand (COD) of industrial wastewater was decreased up to 69.23 % by treatment with $\text{Bi}_2\text{MoO}_6/\text{GO}$ nanoflakes. This is due to the fact that the organic matter/ dye was oxidized in the wastewater. It was concluded that $\text{Bi}_2\text{MoO}_6/\text{GO}$ nanoflakes have good photocatalytic potential and behave as an oxidizing agent for organic species, including dyes, which are present in the industrial wastewater. Nanostructures can oxidize harmful organic species in wastewater and convert them into nontoxic molecules e.g CO_2 and H_2O .

4. CONCLUSION

This study concluded that $\text{Bi}_2\text{MoO}_6/\text{GO}$ composite was synthesized by facile hydrothermal method with dispersed graphene oxide nanosheets. The SEM analysis revealed the sheet-like morphology of GO and flake-like for $\text{Bi}_2\text{MoO}_6/\text{GO}$ composite material. They developed an interfacial interaction during composite formation. This interaction plays a major role to suppress the recombination of electron-hole pairs by promoting the transfer of excited electrons to reduce the adsorbed oxygen on the catalyst surface. Separation of charge carriers prolongs the photogenerated charge carriers leading to the formation of more reactive oxygen species to oxidize the dye molecules. Results showed that flakes like $\text{Bi}_2\text{MoO}_6/\text{GO}$ composite give 99.00 % degradation of DV dye and reduce the 69.23 % reduction of COD for industrial wastewater under the influence of solar light. Results revealed that such nanostructures can be utilized for the

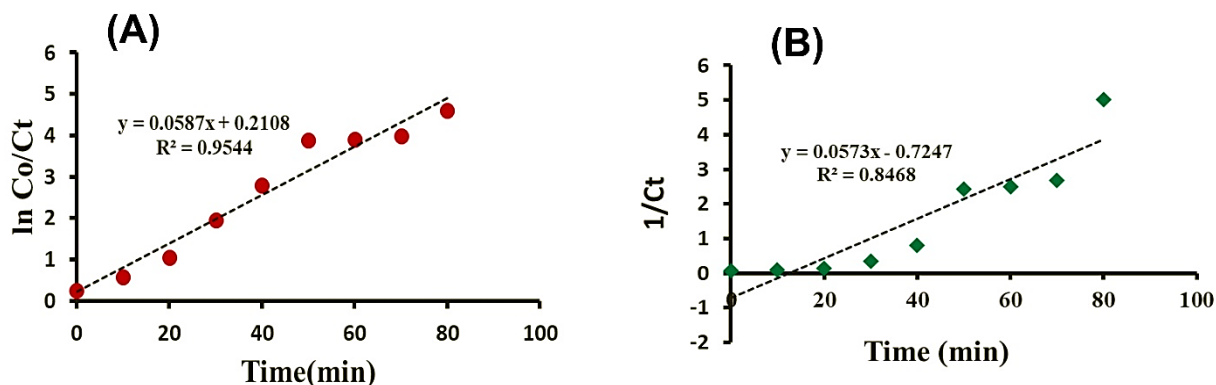


Fig. 6. Pseudo 1st order kinetic modeling, plot between $\ln(C_0/C_t)$ and time (t) for photodegradation of DV dye by the photocatalytic activity of $\text{Bi}_2\text{MoO}_6/\text{GO}$ nanoflakes (A) and plot between $1/C_t$ and time (t) for photodegradation of DV dye by the photocatalytic activity of $\text{Bi}_2\text{MoO}_6/\text{GO}$ nanoflakes (B).

degradation of organic water pollutants on an industrial scale before the discharge of wastewater into water bodies i.e. lakes, rivers, etc. These dyes are harmful to the living species and also to the environment and should be treated before their discharge into the water bodies.

5. ACKNOWLEDGEMENTS

The author acknowledges the financial assistance from the Higher Education Commission (HEC) of Pakistan under the International Research Initiative Support Program (IRSIP).

6. CONFLICT OF INTEREST

There is no conflict of interest.

7. REFERENCES

1. V. Kumar, K.H. Kim, J.W. Park, J. Hong, and S. Kumar. Graphene and its nanocomposites as a platform for environmental applications. *Chemical Engineering Journal* 315: 210–232 (2017).
2. H. Dong, G. Zeng, L. Tang, C. Fan, C. Zhang, X. He, and Y. He. An overview on limitations of TiO_2 -based particles for photocatalytic degradation of organic pollutants and the corresponding countermeasures. *Water research* 79: 128–146 (2015).
3. P.C.L. Muraro, S.R. Mortari, B.S. Vizzotto, G. Chuy, C. Dos Santos, L.F.W. Brum, and W.L. Da Silva. Iron oxide nanocatalyst with titanium and silver nanoparticles: Synthesis, characterization and photocatalytic activity on the degradation of Rhodamine B dye. *Scientific reports* 10: 3055 (2020).
4. A. Sahoo, and S. Patra. A combined process for the degradation of azo-dyes and efficient removal of aromatic amines using porous silicon supported porous ruthenium nanocatalyst. *ACS Applied Nano Materials* 1: 5169–5178 (2018).
5. P.M. Shaibani, K. Prashanthi, A. Sohrabi, and T. Thunda. Photocatalytic BiFeO_3 nanofibrous mats for effective water treatment. *Journal of Nanotechnology* 2013:939531 (2013).
6. M.M. Sajid, S.B. Khan, N.A. Shad, N. Amin, and Z. Zhang. Visible light assisted photocatalytic degradation of crystal violet dye and electrochemical detection of ascorbic acid using a $\text{BiVO}_4/\text{FeVO}_4$ heterojunction composite. *RSC advances* 8: 23489–23498 (2018).
7. M.Y.A. Khan, M. Zahoor, A. Shaheen, N. Jamil, M.I. Arshad, S.Z. Bajwa, N.A. Shad, R. Butt, I. Ali, and M.Z. Iqbal. Visible light photocatalytic degradation of crystal violet dye and electrochemical detection of ascorbic acid & glucose using BaWO_4 nanorods. *Materials Research Bulletin* 104: 38–43 (2018).
8. X. Wang, X. Yao, H. Bai, and Z. Zhang. Oxygen vacancy-rich 2D GO/ BiOCl composite materials for enhanced photocatalytic performance and semiconductor energy band theory research. *Environmental Research* 212: 113442 (2022).
9. M. Iqbal, H.N. Bhatti, S. Younis, S. Rehmat, N. Alwadai, A.H. Almuqrin, and M. Iqbal. Graphene oxide nanocomposite with CuSe and photocatalytic removal of methyl green dye under visible light irradiation. *Diamond and Related Materials* 113: 108254 (2021).
10. Z. Zhu, S. Wan, Y. Zhao, Y. Gu, Y. Wang, Y. Qin, Z. Zhang, X. Ge, Q. Zhong, and Y. Bu. Recent advances in bismuth-based multimetal oxide photocatalysts for hydrogen production from water splitting: Competitiveness, challenges, and future perspectives. *Materials Reports: Energy* 1: 100019 (2021).
11. Z. Du, C. Cui, S. Zhang, H. Xiao, E. Ren, and R. Guo. S. Jiang, Visible-light-driven photocatalytic degradation of rhodamine B using $\text{Bi}_2\text{WO}_6/\text{GO}$ deposited on polyethylene terephthalate fabric. *Journal of Leather Science and Engineering* 2: 16 (2020).
12. W.S. Hummers Jr, and R.E. Offeman. Preparation of graphitic oxide. *Journal of the American Chemical Society* 80: 1339 (1958).
13. J. Li, T. Tao, X.b. Li, J.l. Zuo, T. Li, J. Lu, S.h. Li, L.z. Chen, C.y. Xia, and Y. Li. A spectrophotometric method for determination of chemical oxygen demand using home-made reagents. *Desalination* 239: 139–145 (2009).
14. S.C. Ray. Application and uses of graphene oxide and reduced graphene oxide: in book Applications of graphene and graphene-oxide based nanomaterials 1st ed. pp. 39–55 (2015).
15. S. Maswanganyi, R. Gusain, N. Kumar, E. Fosso-Kankeu, F.B. Waanders, and S.S. Ray. Bismuth molybdate nanoplates supported on reduced graphene oxide: an effective nanocomposite for the removal of naphthalene via adsorption–photodegradation. *ACS omega* 6: 16783–16794 (2021).
16. L. Feng, D. Yang, S. Gai, F. He, G. Yang, P. Yang, and J. Lin. Single bismuth tungstate nanosheets

- for simultaneous chemo-, photothermal, and photodynamic therapies mediated by near-infrared light. *Chemical Engineering Journal* 351: 1147–1158 (2018).
17. N.M. El-Shafai, M.E. El-Khouly, M. El-Kemary, M.S. Ramadan, and M.S. Masoud. Graphene oxide–metal oxide nanocomposites: fabrication, characterization and removal of cationic rhodamine B dye. *RSC advances* 8: 13332 (2018).
 18. Z. Zhu, S. Wan, Y. Zhao, Y. Gu, Y. Wang, Y. Qin, Z. Zhang, X. Ge, Q. Zhong, and Y. Bu. Recent Advances in Bismuth-Based Multimetal Oxide Photocatalysts for Hydrogen Production from Water Splitting: Competitiveness, Challenges, and Future Perspectives. *Materials Reports: Energy* 1: 100019 (2021).
 19. S. Maswanganyi, R. Gusain, N. Kumar, E. Fosso-Kankeu, F.B. Waanders, and S.S. Ray. Bismuth Molybdate Nanoplates Supported on Reduced Graphene Oxide: An Effective Nanocomposite for the Removal of Naphthalene via Adsorption–Photodegradation. *ACS Omega* 6:16783–16794 (2021).
 20. N. Lv, Y. Li, Z. Huang, T. Li, S. Ye, D.D. Dionysiou, and X. Song. Synthesis of GO/TiO₂/Bi₂WO₆ nanocomposites with enhanced visible light photocatalytic degradation of ethylene. *Applied Catalysis B: Environmental* 246: 303–311 (2019).
 21. S. Ahmadi, A. Rahdar, C.A. Igwegbe, S. Mortazavi-Derazkola, A.M. Banach, S. Rahdar, A.K. Singh, S. Rodriguez-Couto, and G.Z. Kyzas. Praseodymium-doped cadmium tungstate (CdWO₄) nanoparticles for dye degradation with sonocatalytic process. *Polyhedron* 190: 114792 (2020).
 22. E.S. Mansor, F.N. El Shall, and E.K. Radwan. Simultaneous decolorization of anionic and cationic dyes by 3D metal-free easily separable visible light active photocatalyst. *Environmental Science and Pollution Research* 9:1–14 (2022).
 23. M.M. Sajid, N.A. Shad, Y. Javed, S.B. Khan, N. Amin, Z. Zhang, Z. Imran, and M.I. Yousuf. Facile synthesis of Zn₃(VO₄)₂/FeVO₄ heterojunction and study on its photocatalytic and electrochemical properties. *Applied Nanoscience* 10: 421–433 (2020).